ACS APPLIED MATERIALS & INTERFACES

Research Article

Cite This: ACS Appl. Mater. Interfaces 2018, 10, 8296−8306

www.acsami.org

Highly Stretchable DNA/Clay Hydrogels with Self-Healing Ability

Ahmet T. Uzumcu, Orhan Guney,* and Oguz Okay*

Departments of Chemistry and Polymer Science & Technology, Istanbul Technical University, Maslak, 34469 Istanbul, Turkey

Supporting Information

ABSTRACT: We present mechanically strong and self-healable clay hydrogels containing 2−8 w/v % ds-DNA together with a synthetic biocompatible polymer, poly(*N*,*N*-dimethylacrylamide). Clay nanoparticles in the hydrogels act like a chemical cross-linker and promote their elastic behavior, whereas DNA contributes to their viscoelastic energy dissipation. The extent of mechanical hysteresis during cyclic tensile tests reveals that the strength of intermolecular bonds in DNA/clay hydrogels is in the range of the strength of hydrogen bonds. The hydrogels exhibit a high stretchability (up to 1500%) and a tensile strength between 20 and 150 kPa. They have the ability to self-heal, which is induced by heating the damaged gel samples above the melting temperature of ds-DNA. When comparing the mechanical properties of the hydrogels before and after healing, the healing efficiency is greater than 100%. We also demonstrate that ds-DNA molecules entrapped in the gel network undergoes thermal denaturation/renaturation cycles, leading to a further improvement in the mechanical properties of the hydrogels.

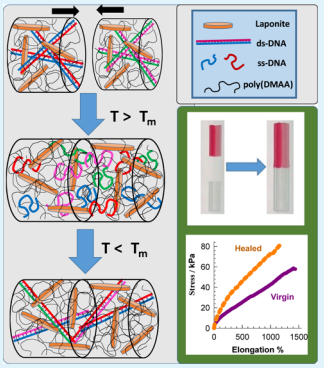

KEYWORDS: *DNA, clay, nanocomposite hydrogels, mechanical properties, self-healing*

INTRODUCTION

Deoxyribonucleic acid (DNA) existing in all living cells is a semiflexible biopolymer with a double-helical conformation in its native state. Heating aqueous double-stranded (ds) DNA solutions breaks the hydrogen bonds keeping the double strands together, and ds-DNA dissociates into flexible single strands.[1] The thermal transition from double-to-single-stranded (ss) DNA is called denaturation or melting, which can be reversed by slow cooling dilute DNA solutions.[2] DNA as a smart biomaterial has received interest in the past decades because of its programmable base-pairing recognition, designable sequence, and predictable secondary structure.[3,4] Hydrogels derived from DNA are 3D networks of DNA strands containing large quantities of water.[5,6] DNA hydrogels are excellent candidates to utilize the unique features of DNA molecules, such as bioresponsivity, biocompatibility, biodegradability, selective binding, and molecular recognition.[7,8] DNA-based hydrogels can thus be used in a variety of applications including controlled release of biocatalysts,[9] chemotherapy drug doxorubicin,[10] proteins,[11] and cells;[12] for constructing three-dimensional tissuelike structures;[13] and for highly sensitive detection of mercury and lead ions,[14−16] cocaine,[16] and DNA.[17]

Several approaches have been developed to produce physical or chemical DNA hydrogels.[3,4,9,11,18−23] For instance, a chemical network of DNA strands was created by enzymatic ligation of branched DNA,[24] whereas DNA hydrogels with reversible cross-links were produced by cross-linking DNA−polyethylene glycol−DNA triblock copolymers using K^+ or Na^+ ions.[25] Liu and co-workers developed several strategies for the preparation of supramolecular DNA hydrogels with self-healing ability.[3,19,21,26] The research group also reported the preparation of double-network hydrogels based on DNA that exhibit a storage modulus of around 300 Pa and reversible gel−sol transition.[20] Supramolecular self-healable graphene oxide/DNA hydrogels exhibiting a storage modulus of 4.6 kPa were also prepared via $\pi-\pi$ stacking and hydrophobic interactions.[18] DNA hydrogels can also be produced by cross-linking DNA in semidilute aqueous solutions in the presence of diepoxides as a chemical cross-linker.[27,28] Despite their many advantages, widespread use of DNA hydrogels is limited because of their poor mechanical properties. Moreover, many applications require mechanically strong DNA hydrogels combined with self-healing ability to prolong their lifetimes.

Physical gels formed by clay such as Laponite nanoparticles provide a protective environment for biomolecules by enhancing their bioresponsivity and stability against degradation, which may have been important in the origin and sustainability of life on earth.[29,30] For instance, ds-DNA without the protection of clay hydrogels is easily digested by the DNase, whereas in the clay environment, it is effectively protected from DNase digestion and preserves its biological function.[29] Laponite is a synthetic hectorite clay that forms disklike particles in water with a thickness of 1 nm and a diameter of about 25 nm stabilized by their surface charges. Haraguchi et al. showed that Laponite particles act as a multifunctional cross-linker during the solution polymerization of monomers such as *N*-isopropylacrylamide (NIPAM) or *N*,*N*-dimethylacrylamide (DMAA) and produce synthetic hydrogels with extraordinary mechanical properties.[31−34] Taki et al. reported a significant increase of the loss factor tan δ after incorporation of DNA in clay hydrogels.[35] Recently, we prepared DNA hydrogels

Received: January 4, 2018
Accepted: February 14, 2018
Published: February 14, 2018

DOI: 10.1021/acsami.8b00168
ACS Appl. Mater. Interfaces 2018, 10, 8296−8306

containing Laponite particles and poly(NIPAM) chains exhibiting a fracture stress and an elongation at break of up to 53 kPa and 544%, respectively.[36] However, they lack the ability to self-heal upon damage, and thermal denaturation/renaturation cycle of ds-DNA in the hydrogel could not be monitored because poly(NIPAM) turns into a collapsed state above its lower critical solution temperature (34 °C).

To address this problem, we present here DNA/clay hydrogels of high stretchability (up to 1500%) and a tensile strength between 20 and 150 kPa by in situ polymerization of DMAA in aqueous solutions of ds-DNA (2−8 w/v %) in the presence of Laponite nanoparticles. The hydrogels thus prepared also contain poly(DMAA), which is a hydrophilic and biocompatible polymer with associative properties.[37,38] As will be seen below, DNA entrapped in clay hydrogels undergoes thermal denaturation/renaturation cycle, leading to a further improvement in the hydrogel mechanical properties. The hydrogels have the ability to self-heal, induced by heating the damaged gel samples above the melting temperature of ds-DNA. When comparing the mechanical properties of the hydrogels before and after healing, the healing efficiency is greater than 100%.

EXPERIMENTAL PART

Materials. The hydrogels were prepared from DNA sodium salt from salmon testes (DNA, Sigma-Aldrich) having a melting temperature of 87.5 °C and an average molecular weight of 1.3×10^6 g/mol corresponding to ∼2000 base pairs. Laponite XLG clay, $[Mg_{5.34}Li_{0.66}Si_8O_{20}(OH)_4]Na_{0.66}$, was purchased from Rockwood Ltd. DMAA provided by Sigma-Aldrich was purified by filtering through activated alumina. Ammonium persulfate (APS), *N*,*N*,*N*′,*N*′-tetramethylethylenediamine (TEMED), and ethidium bromide (EtBr) were all purchased from Sigma-Aldrich (St Lois, MO) and used without purification.

Hydrogel Preparation. The hydrogels were prepared at 25 °C by polymerization of 1 M DMAA in aqueous ds-DNA solutions containing Laponite XLG clay in the presence of an APS (3.5 mM)—TEMED (0.08 v/v %) redox initiator system. Two sets of experiments were carried out. In the first set, clay content was varied between 2 and 7 w/v % at 2 w/v % DNA. In the second set, the clay content was kept at 5 w/v %, whereas the concentration of DNA was varied between 2 and 8 w/v %, which are much above its critical overlap concentration (0.043 w/v %).[27] Laponite clay was first dispersed in deionized water under vigorous stirring for 60−90 min to obtain a homogeneous transparent dispersion. After addition of DMAA and mixing for 15 min, ds-DNA was included in the solution and stirred for 24 h at 35 °C. The initiator APS was then added to the viscous solution and stirred in an ice-water bath for 1 h, followed by the addition of the accelerator TEMED to initiate the reaction. The reaction solutions were transferred into plastic syringes of 4.5 mm in internal diameter as well as between parallel plates of the rheometer to monitor the gelation reactions. To highlight the effect of DNA on the gel properties, the hydrogels were also prepared without addition of ds-DNA.

Fluorescence Measurements. The measurements were carried out using a Varian Cary-Eclipse Luminesce spectrometer. The gelation solutions containing 10 μM ethidium bromide (EtBr) as a fluorescent probe were transferred into the fluorescence cell of the spectrometer, which is a cylindrical glass tube of 10 mm in internal diameter. The measurements were performed at various reaction times at an excitation wavelength of 530 nm, and then, the emission spectra between 550 and 800 nm were recorded. For the measurements on hydrogel samples at various temperatures between 25 and 90 °C, they were first immersed in a temperature-controlled water bath to adjust the temperature prior to the measurements.

Rheological Experiments. Rheological tests were carried out on a Bohlin Gemini 150 rheometer system (Malvern Instruments, UK) equipped with a Peltier device for temperature control. The gelation solutions were placed between the parallel plates of the instrument. The upper plate (diameter, 40 mm) of the rheometer was set at a distance of 500 μm before the onset of the reactions. During all of the rheological tests, a solvent trap was used and the outside of the upper plate was covered with a thin layer of low-viscosity silicone oil to prevent evaporation of water. The dynamic moduli of the reaction system were monitored at a frequency ω = 6.28 rad s^{-1} and a deformation amplitude γ_o = 0.01 to ensure that the oscillatory deformation is within the linear regime (Figure S1). After a reaction time of 2 h, frequency-sweep tests at γ_o = 0.01 were carried out at 25 °C over the frequency range 6.3×10^{-2} to 3.1×10^2 rad s^{-1}. Oscillatory deformation tests on gel samples were also carried out by on−off switching of the applied strain γ_o. The tests were carried out by application of a high strain and monitoring the dynamic moduli of the sample for a duration of 10 min, followed by immediate reduction of the strain to a low value and monitoring the moduli for 10 min. The gel samples formed between the parallel plates of the rheometer were also subjected to thermal cycles by first heating from 25 to 90 °C at a rate of 3.3 °C·min^{-1}, keeping at 90 °C for 10 min, then cooling back to 25 °C at 1.1 °C·min^{-1}, and finally keeping at 25 °C for at least 10 min. The changes in the dynamic moduli of the gels were monitored during the course of the cycle as a function of temperature.

X-ray Diffraction Measurements. The hydrogel samples were dried at 24 ± 1 °C for 48 h and then at 80 °C under vacuum for 24 h. X-ray diffraction (XRD) patterns of dried gel samples were collected on a Bruker AXS D8 diffractometer using a Cu Kα source (λ = 1.54184 Å) operated at 30 kV/10 mA. The patterns were collected in the 5−15° 2θ range at a scan rate of 0.01°·min^{-1}.

Mechanical Tests. Uniaxial elongation tests were performed on a Zwick Roell Z0.5 TH test machine using a 500 N load cell. The tests were carried out at 24 ± 1 °C using cylindrical gel samples of about 4.5 mm in diameter. The initial sample length between jaws was fixed at 30 ± 2 mm. The nominal stress σ_{nom} and strain ε, which is the change in the sample length relative to its initial length, were recorded at a fixed strain rate of 5.6×10^{-2} s^{-1}. The Young's modulus E was calculated from the slope of stress−strain curves between 5 and 15% deformations. Cyclic elongation tests were conducted by first stretching the gel sample to a maximum strain ε_{max} and then unloading. After certain relaxation time which was varied between 3 and 9 min, they were again stretched to a higher ε_{max} that increased stepwise from 200 to 800%. To quantify the self-healing ability of the hydrogels, gel samples were cut in the middle, and then the two halves were gently connected together within a plastic syringe (having the same diameter as the samples), followed by heating to 80 or 90 °C. To quantify the healing efficiency, uniaxial elongation tests were performed on both virgin and healed gel samples.

Swelling Tests and DNA Release Studies. DNA/clay hydrogels of about 4.5 mm in diameter were cut into samples of about 10 mm in length. Each gel sample of mass m_o was immersed in an excess of water, and the gel mass m in water at 24 ± 0.5 °C was monitored by weighing the samples every day and refreshing water. The relative degree of swelling $m_{rel} = m/m_o$ was monitored until obtaining the equilibrium swelling degree $m_{rel,eq}$. For accurate results, at least three different samples were measured for each type of gel. The amount of ds-DNA released during swelling was estimated by both UV and fluorescence spectroscopies. For UV measurements, ds-DNA release to water was monitored on a T80 UV−vis spectrometer using the molar extinction coefficient ε_{260} determined as 6900 M^{-1} cm^{-1} at 260 nm. For the fluorescence measurements, water samples were collected from the external solution during the swelling process of the hydrogels. After addition of 10 μM EtBr, the measurements were conducted at an excitation wavelength of 530 nm, and then, the emission spectra between 550 and 800 nm were recorded. The amount of ds-DNA released from the hydrogels was estimated from the maximum intensity at 600 nm (I_{max}). For this purpose, a calibration curve was prepared by measuring I_{max} of aqueous 10 μM EtBr solutions containing varying amounts of ds-DNA (0−30 mM) and plotting I_{max} against ds-DNA concentration.

DOI: 10.1021/acsami.8b00168
ACS Appl. Mater. Interfaces 2018, 10, 8296−8306

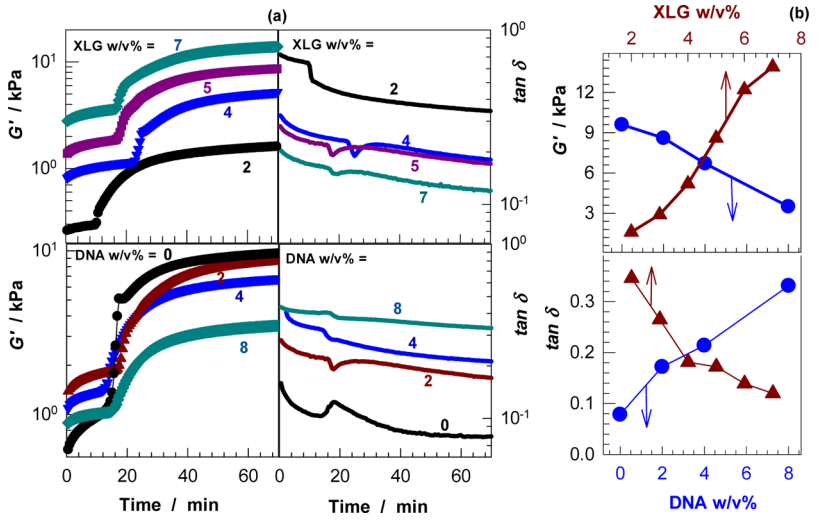

Figure 1. (a) Variations of the storage modulus G' and the loss factor tan δ during the formation of NC-DNA hydrogels. The data are from the first (upper panel) and second sets of experiments (bottom panel). Temperature = 25 °C. ω = 6.3 rad s^{-1}. γ_o = 0.01. (b) G' and tan δ of the hydrogels after a reaction time of 70 min plotted against their DNA (circles) and XLG contents (triangles).

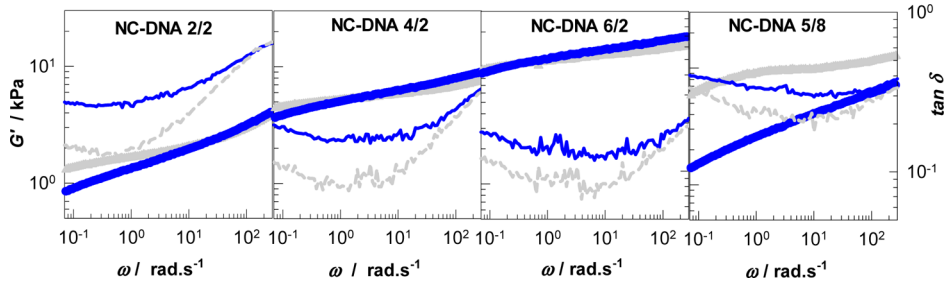

Figure 2. G' (blue circles) and tan δ (solid curves) of NC-DNA hydrogels shown as a function of frequency ω measured after 2 h of reaction time. The hydrogel codes are indicated. G' and tan δ of the corresponding NC hydrogels are shown by gray triangles and dashed curves, respectively. Temperature = 25 °C. γ_o = 0.01.

RESULTS AND DISCUSSION

Formation and Microstructure. DNA/clay hydrogels were prepared by free-radical polymerization of DMAA at a concentration of 1 M in aqueous ds-DNA solutions containing Laponite (XLG) nanoparticles. Two sets of gelation experiments were carried out. In the first set, the amount of DNA in the feed was set to 2 w/v %, whereas the XLG content was varied between 2 and 7 w/v %. In the second set, the XLG content was kept at 5 w/v % and DNA concentration was varied between 2 and 8 w/v %. In the following, the hydrogels are denoted as NC-DNA-x/y, where NC means nanocomposite and x and y denote the concentrations of XLG and DNA in w/v %, respectively. For comparison, hydrogels without DNA were also prepared and denoted as NC-x. Figure 1a shows the reaction time dependences of the storage modulus G' and loss factor tan δ ($=G''/G'$) during the first (upper panel) and second sets of experiments (bottom panel). Following an induction period of 14 ± 4 min, the modulus G' rapidly increases while tan δ decreases, and then, they approach plateau values after about 70 min. Figure 1b showing G' and tan δ values after a reaction time of 70 min reveals the opposite effects of DNA and XLG on the viscoelastic properties of NC-DNA hydrogels. XLG acts like a chemical cross-linker and promotes the elastic behavior of the hydrogels by increasing the modulus and decreasing the loss factor. In contrast, DNA contributes to their viscoelasticity and produces hydrogels with a lower modulus and a higher loss factor, suggesting the weakening of clay−polymer interactions in the presence of DNA.

Figure 2 shows the frequency dependences of G' (blue circles) and tan δ (solid curves) for NC-DNA hydrogels after a reaction time of 2 h. For comparison, G' and tan δ of the corresponding NC hydrogels prepared without DNA are also shown by gray triangles and dashed curves, respectively. The general trend is that at low frequencies, NC-DNAs exhibit a lower modulus and a higher loss factor as compared to the NCs, revealing energy dissipation. We attribute this energy dissipation on long experimental time scales to the weak clay/DNA interactions. ds-DNA molecules in the hydrogel could follow the slow oscillation and slip on the surface of the nanoparticles by dissipating energy. At high frequencies, tan δ of NC-DNAs is similar to that of NCs, likely because the semiflexible ds-DNA with a persistence length of 50 nm could not move with a high frequency in the gel network.

The results can be explained by considering the extent of intermolecular interactions between the gel components. XLG nanoparticles suspended in water carry strongly negative charge on their surface and weakly positive charge on their rim.[39,40] Previous work shows that nonionic monomers such as DMAA surround the surface of XLG particles in aqueous solutions, which prevents the formation of clay hydrogels with a house-of-cards structure via face−rim associations.[31,33,41−43] After polymerization of DMAA in aqueous XLG dispersion, a large number of poly(DMAA) chains are aggregated on the surface

DOI: 10.1021/acsami.8b00168
ACS Appl. Mater. Interfaces 2018, 10, 8296−8306

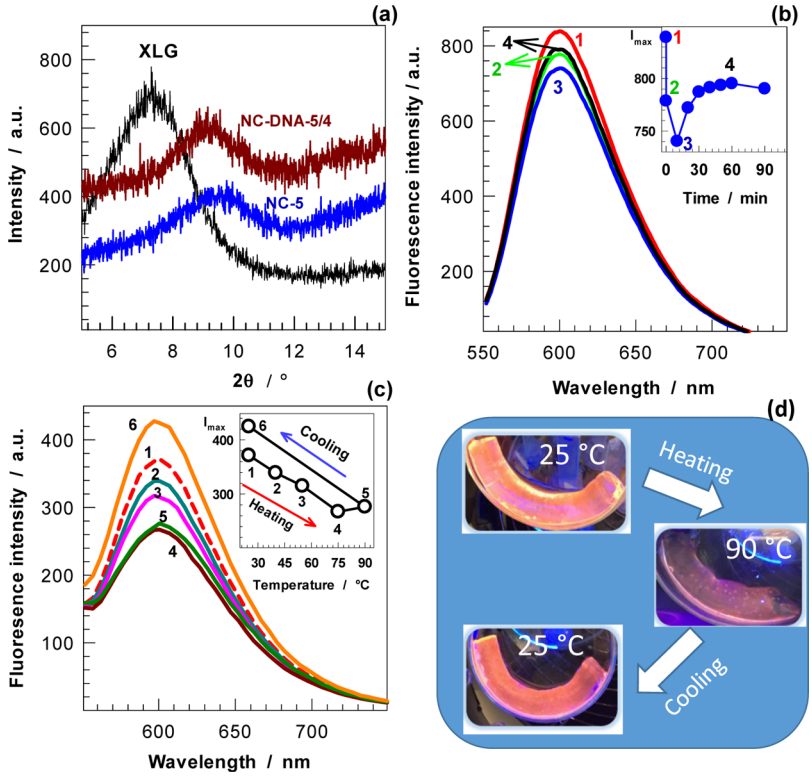

Figure 3. (a) XRD patterns of XLG, dried NC-DNA-5/4, and NC-5 hydrogels in 5−15° 2θ ranges. Scan rate = 0.01°·min^{-1}. (b) Fluorescence spectra of 10 μM EtBr in gelation solution containing 1 M DMAA, 2 w/v % DNA, and APS/TEMED redox initiator system. The spectra were recorded before and after addition of APS/TEMED initiator system and after reaction times of 10 and 60 min, indicated by 1, 2, 3, and 4, respectively. The inset shows the emission intensity of EtBr at 600 nm plotted against the reaction time. (c) Fluorescence spectra of EtBr in NC-DNA-5/4 hydrogel at 25 (1), 40 (2), 55 (3), 75 (4), and 90 °C (5) and after cooling back to 25 °C (6). The inset shows the emission intensity of EtBr at 600 nm plotted against the temperature. The numbers in the inset correspond to those given on the spectra. Note that the slight increase of the intensity between points 4 and 5 was not observed in the absence of XLG (Figure S2). (d) Images of NC-DNA-5/4 hydrogel sample swollen in 10 μM EtBr solution. The images were taken under UV light at 25 and 90 °C and after cooling back to 25 °C.

of clay particles, which form multiple hydrogen bonding with the particles, leading to hydrogels with extraordinary mechanical properties.[31] However, DNA cannot surround the particles because of its repulsive interactions with the negatively charged particle surfaces, which prevent hydrogen bonding between DNA and clay so that DNA strands can slip between the particles by dissipating energy. Thus, increasing amount of DNA in the hydrogel also increases the loss factor because of the weak DNA/clay interactions.

The surface charge of XLG clay used in the hydrogel preparation provides homogeneous distribution of clay nanoparticles in deionized water as well as in DMAA solutions with an exfoliated structure.[31−34] To demonstrate the exfoliation of XLG in the viscous gelation solution containing ds-DNA of 2000 base pairs long, XRD measurements were carried out on dried gel samples. Figure 3a shows the XRD patterns of dried NC-DNA-5/4 and NC-5 hydrogels together with that of XLG clay as a reference. The clay shows a strong diffraction peak at 2θ = 7.2° corresponding to a layer spacing of 1.23 nm between regularly stacked clay sheets. This peak is absent in both NC-DNA-5/4 and NC-5 hydrogels, indicating that the clay particles are dispersed uniformly throughout the poly(DMAA)/DNA network, similar to the ordinary NC hydrogels prepared without DNA.

Another question regarding the microstructure of NC-DNA hydrogels is whether the native ds conformation of DNA remains intact after the gelation reaction or ds-DNA dissociates into single strands? To monitor the conformation of DNA during gelation, fluorescence measurements were conducted using ethidium bromide (EtBr) as a fluorescent probe. EtBr is known to bind ds-DNA by intercalation of its planar phenanthridium ring between the DNA base pairs and results in an increase of EtBr fluorescence.[28,44] Because of the intercalation mechanism, ds-DNA leads to a higher increase in EtBr intensity than ss DNA. Figure 3b shows the fluorescence spectra of 10 μM EtBr in a gelation solution containing 1 M DMAA, 2 w/v % DNA, and APS/TEMED redox initiator system. Because XLG nanoparticles interact with EtBr and result in an enhancement of EtBr fluorescence intensity,[36] XLG was not included in the gelation solution. The spectra were recorded before and just after the addition of APS/TEMED initiator system and after reaction times of 10 and 60 min, indicated in Figure 3b by 1, 2, 3, and 4, respectively. The inset of the figure shows the emission intensity of EtBr at 600 nm plotted against the reaction time up to 90 min.

The emission intensity of EtBr rapidly decreases after the addition of APS/TEMED system as well as during the induction period of the reaction (Figure 1a), and it again increases with increasing reaction time up to 40 min and then levels off. We attribute the initial decrease of the fluorescence intensity to the interactions between negatively charged sulfate groups of APS and the positively charged phenanthridium ring nitrogen of EtBr.[45] However, after gel formation, ionic

DOI: 10.1021/acsami.8b00168
ACS Appl. Mater. Interfaces 2018, 10, 8296−8306

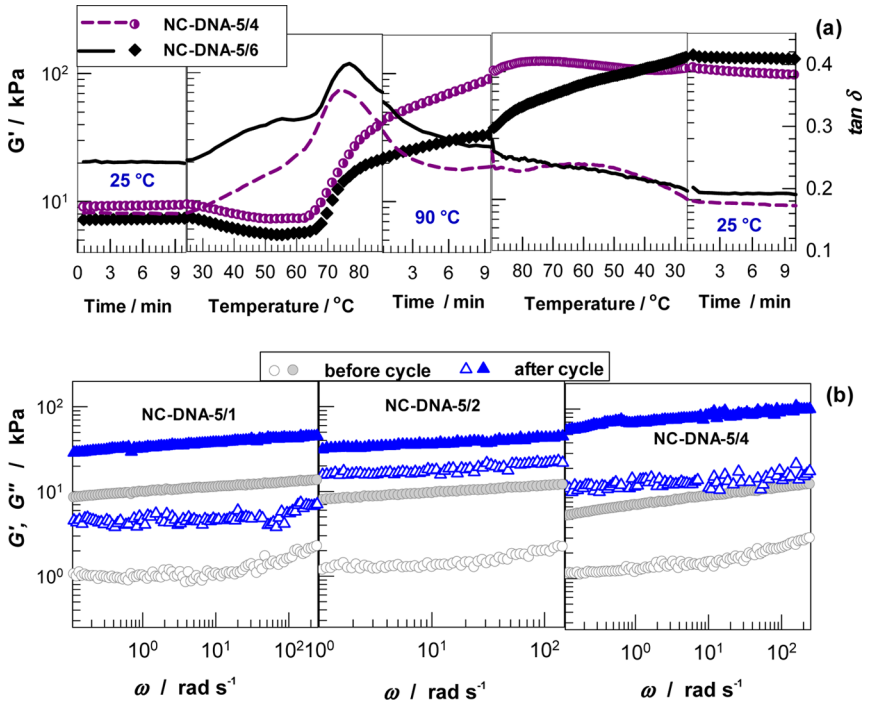

Figure 4. (a) G' (symbols) and tan δ (lines) of NC-DNA-5/4 and NC-DNA-5/6 hydrogels during heating−cooling cycle between 25 and 90 °C. ω = 6.28 rad s^{-1}. γ_o = 0.01. (b) Frequency dependence of G' (filled symbols) and G'' (open symbols) for NC-DNA hydrogels before and after the heating−cooling cycle. Temperature: 25 °C. γ_o = 0.01.

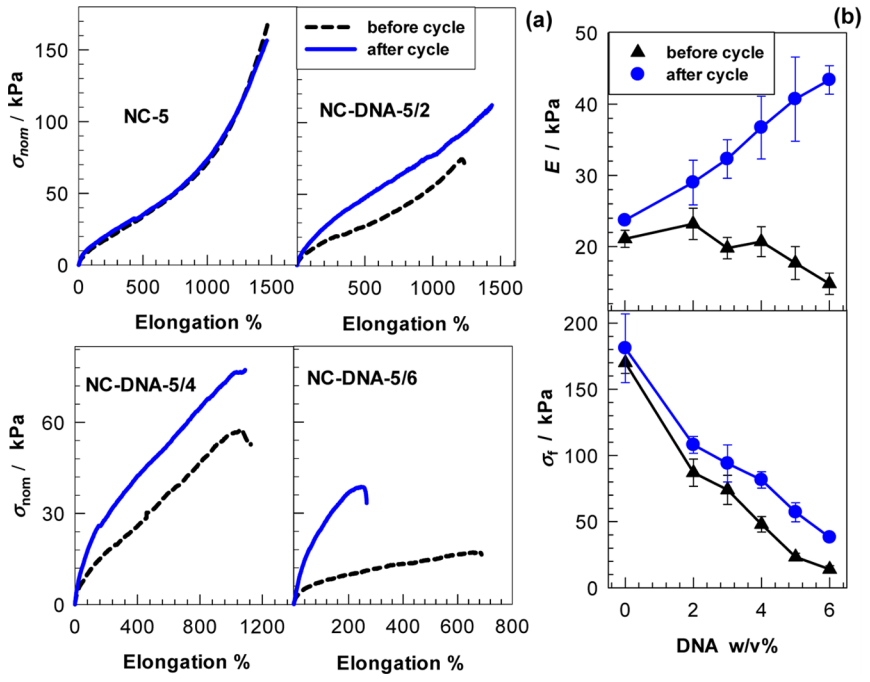

Figure 5. (a) Nominal stress σ_{nom} plotted against the elongation ratio ε of NC-DNA and NC hydrogels before (dashed curves) and after the heating−cooling cycle (solid curves). Strain rate = 5.6×10^{-2} s^{-1}. Temperature = 24 ± 1 °C. (b) Young's modulus E and the fracture stress σ_f of the hydrogels before (triangles) and after the heating−cooling cycle (circles) plotted against their DNA contents.

interactions between EtBr and APS become weaker because of the intercalation of EtBr between the base pairs of DNA within the gel network so that the intensity again increases.[46]

The stability of native DNA conformation in the hydrogels was also verified by subjecting NC-DNA gel specimens after a reaction time of 24 h to the heating−cooling cycles between below and above the melting temperature T_m (87.5 °C) of ds-DNA. Sealed hydrogel samples containing 10 μM EtBr were first heated from 25 to 90 °C at a heating rate of 3.25 °C·min^{-1} and then cooled back at 1.1 °C·min^{-1} during which the emission spectra were recorded. Figure 3c shows the typical fluorescence spectra of EtBr in NC-DNA-5/4 hydrogel at various temperatures, and the inset presents the emission intensity of EtBr at 600 nm plotted against the temperature.

DOI: 10.1021/acsami.8b00168
ACS Appl. Mater. Interfaces 2018, 10, 8296−8306

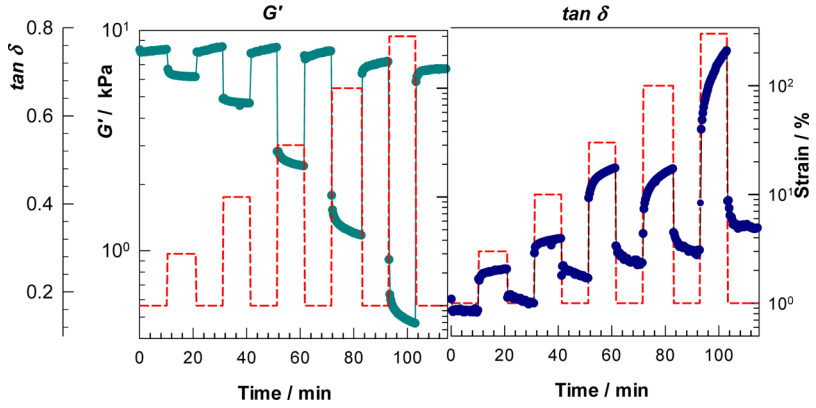

Figure 6. G' (left) and tan δ (right) of NC-DNA-5/4 hydrogel during the on−off strain cycles plotted against time. The dashed red lines represent the schedule of the stepwise increased strain $\gamma_{o,h}$ separated with a low strain $\gamma_{o,l}$. Temperature = 25 °C.

The numbers on the spectra correspond to the numbers shown in the inset. The maximum intensity decreases as the temperature is increased to 90 °C, indicating the conformational transition from ds- to ss-DNA within the hydrogel and thus confirming that DNA is in its native conformation after gelation. When the gel is cooled back to 25 °C, the fluorescence emission intensity of EtBr in the gel again increases and rises above its initial value (Figure 3c). When the experiments were repeated using hydrogel samples prepared without XLG, the fluorescence intensity after the heating−cooling cycle returned back close to the initial value, revealing that the clay nanoparticles are responsible for the higher intensity (Figure S2). The conformational transition of ds-DNA in the hydrogels was also visualized by the optical images of the gel samples swollen in 10 μM EtBr solution (Figure 3d). The initial yellow-orange color of the gel specimen under UV light becomes weaker at 90 °C because of the decrease of the fluorescence intensity, and the initial color is recovered upon cooling to 25 °C. The results thus reveal that upon heating above T_m, ds-DNA molecules in NC-DNA hydrogels are dissociated into single strands and this can be reversed by cooling below the melting temperature T_m.

Previous work shows that the storage modulus G' of aqueous semidilute solutions of ds-DNA significantly increases when subjected to the heating−cooling cycles between below and above the melting temperature of DNA.[27,28,47] This phenomenon is due to the formation of hydrogen bonds between strands belonging to different ds-DNA molecules acting as additional physical cross-links. We observed a similar behavior in the present NC-DNA hydrogels, as presented in Figure 4a, where the variations of G' and tan δ of NC-DNA-5/4 and NC-DNA-5/6 hydrogels are shown during the heating−cooling cycle between 25 and 90 °C. Figure 4b shows the frequency-sweep results of NC-DNA-5/1, NC-DNA-5/2, and NC-DNA-5/4 hydrogels before (gray circles) and after the heating−cooling cycle (blue triangles). tan δ significantly increases during the heating period, reflecting energy dissipation due to the dissociation of semiflexible ds-DNA to its flexible single strands. Moreover, G' increases about 1 order of magnitude after the cycle, indicating the formation of additional hydrogen bonds. The final modulus of the hydrogels is in the range of 100 kPa and remained almost unchanged at room temperature. In contrast, NC hydrogels prepared without DNA showed a much lesser extent of modulus increase after the cycle, and this increase was reversible; that is, G' dropped back close to its initial value after a storage time of 7 h (Figure S3).

Mechanical Properties and Self-Healing Behavior. Mechanical properties of NC-DNA hydrogels were investigated at 24 ± 1 °C by uniaxial elongation and compression tests. Because of the significant effect of the heating−cooling cycle between below and above T_m of ds-DNA on the hydrogel properties, the tests were carried out on the gel specimens before and after subjecting to the thermal cycles. Figure 5a shows the typical tensile stress−strain curves at a strain rate of 5.6×10^{-2} s^{-1} for NC-DNA-5/2, NC-DNA-5/4, and NC-DNA-5/6 hydrogels before (dashed curves) and after subjecting to the heating−cooling cycles (solid curves). For comparison, the data obtained from NC-5 hydrogel containing no DNA are also shown. As expected, stress−strain curves of NC-5 hydrogel before and after the cycle are similar. In contrast, all NC-DNAs after the cycle exhibit a higher initial slope, that is, Young's modulus E, and a higher fracture stress σ_f as compared to those of the virgin ones.

The modulus E and the fracture stress σ_f of the hydrogels compiled in Figure 5b reveal that the higher the DNA content, the higher the increase of both the modulus and the fracture stress after the thermal cycle, reflecting the formation of additional physical cross-links due to the denaturation and renaturation of ds-DNA. Similar results were also obtained from uniaxial compression tests (Figure S4). Moreover, the stretchability of NC-DNA hydrogels is between 140 and 800% at or above 4 w/v % DNA, whereas it significantly increases with decreasing DNA content. Highly stretchable hydrogels exhibiting an elongation at break between 1100 and 1500% could be obtained at 1−4 w/v % DNA (Figures 5a and S5).

Because of the supramolecular nature of the hydrogels, they are potential candidates for self-healing systems. To understand whether the intermolecular noncovalent bonds dissociate and reassociate reversibly under stress, rheological and mechanical tests were conducted on NC-DNA hydrogels. The gel samples in the form of membranes of 0.5 mm in thickness located between the parallel plates of the rheometer were subjected to oscillatory deformation tests by on−off switching of the applied strain γ_o. The tests consisted of the application of a high strain $\gamma_{o,h}$ and monitoring the storage G' and loss moduli G'' of the gel sample for a duration of 10 min, followed by immediate reduction of $\gamma_{o,h}$ to a low value $\gamma_{o,l}$, and monitoring G' and G'' for 10 min. $\gamma_{o,l}$ was fixed at 1%, whereas $\gamma_{o,h}$ was stepwise increased from 3 to 300%.

The results for NC-DNA-5/4 hydrogel are shown in Figure 6, where the storage modulus G' (left) and the loss factor tan δ (right) during the repeated on−off strain cycles are plotted

DOI: 10.1021/acsami.8b00168
ACS Appl. Mater. Interfaces 2018, 10, 8296−8306

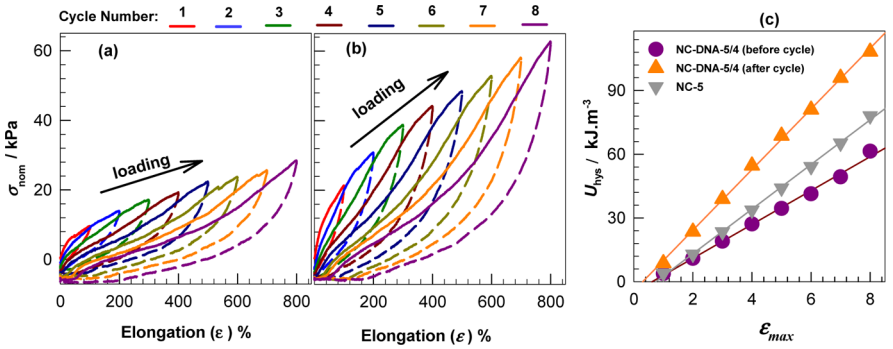

Figure 7. (a,b) Nominal stress σ_{nom} vs elongation ratio ε curves from cyclic elongation tests of NC-DNA-5/4 hydrogels before (a) and after the heating−cooling cycle (b). The tests were conducted with increasing maximum strain ε_{max} with a waiting time of 9 min between cycles. Temperature = 24 ± 1 °C. (c) Hysteresis energies U_{hys} of NC-DNA-5/4 before (circles) and after the heating−cooling cycle (triangles up) and NC-5 (triangles down) shown as a function of maximum strain ε_{max}. The lines are best fit to the data.

against time. The dashed red lines represent the schedule of the stepwise increased $\gamma_{o,h}$ separated with a low strain $\gamma_{o,l}$ of 1%. Upon application of a high strain, the modulus G' decreases, whereas the loss factor tan δ increases, indicating the damage in the gel sample and energy dissipation under strain. However, when the strain is reduced to $\gamma_{o,l}$, G' again increases and tan δ decreases, revealing the recovery of the microstructure. For instance, G' of the hydrogel under 300% strain is 0.5 kPa, whereas after reducing the strain to 1%, G' increases to 6.7 kPa, which is 84% of the modulus of the virgin gel sample (8 kPa). Figure 6 also shows that the recovery in tan δ is much lower than that in G' and it increases from 0.16 to 0.35 after the repeated strain cycles. The results thus indicate a partial recovery of the initial microstructure of the gel network upon application of a strain up to 300%.

For a deeper understanding of the nature of noncovalent bonds, NC-DNA hydrogels were subjected to cyclic tensile tests at a strain rate of 5.6×10^{-2} s^{-1}. Figure 7a,b shows the cyclic tensile stress−strain curves of NC-DNA-5/4 hydrogels before and after the thermal cycle, respectively. The mechanical cycles comprise eight successive loading (solid curves) and unloading cycles (thin dashed curves) with a relaxation time of 9 min between cycles. Note that in the preliminary experiments, the relaxation time between cycles was varied between 3 and 9 min and the highest recovery was observed after 9 min (Figure S6). The gel samples were first stretched to a maximum strain ε_{max} of 100% and then unloaded. After a waiting time of 9 min, they were again stretched to a higher ε_{max}, which increased stepwise from 200 to 800%. Each cycle shows a mechanical hysteresis that increases with increasing maximum strain ε_{max}. Moreover, the loading curve of each cycle is between the loading and unloading curves of the previous cycle, revealing the quasi-reversibility of the successive cycles. This finding is in accord with the results of the rheological tests and indicates that the original microstructure can partially be restored by allowing the damaged hydrogel to rest between cycles for 9 min.

The energy U_{hys} dissipated during the mechanical cycle was calculated from the area between the loading and unloading curves using the equation

$$U_{hys} = \int_0^{\varepsilon_{max}} \sigma_{nom}\, d\varepsilon - \int_{\varepsilon_{max}}^{0} \sigma_{nom}\, d\varepsilon \quad (1)$$

In Figure 7c, U_{hys} energies of NC-DNA-5/4 before and after the thermal cycle and the corresponding NC-5 are plotted against the maximum strain ε_{max}. U_{hys} linearly increases with ε_{max} with a slope that increases from 7.6 ± 0.3 to 14.0 ± 0.2 kJ·m^{-3} after subjecting NC-DNA-5/4 hydrogel to the thermal cycle (Table 1). We assume that U_{hys} is the sum of the dissociation energies of intermolecular noncovalent bonds broken down during the cyclic tests, that is,[48−51]

$$U_{hys} = U_{xl}\nu_e f_v \quad (2)$$

where U_{xl} is the average dissociation energy of intermolecular bonds, ν_e is the total number of such bonds, that is, the cross-link density of the hydrogel, and f_v is the fraction of bonds broken during the tensile cycle. The cross-linking density ν_e of the hydrogels can be estimated from their Young's moduli E given in Figure 5b using the equation[52,53]

$$E = 3\nu_e RT \quad (3)$$

where R and T are in their usual meanings. Equation 3 assumes affine deformation of the network chains, which is a reasonable assumption for the physical gels under study.[42,54] Linearity of U_{hys} versus ε_{max} plots shown in Figures 7c and S7 reveals that the fraction of broken bonds f_v linearly increases with the maximum strain ε_{max}. The slope of U_{hys} versus ε_{max} curve can thus be written as

$$\frac{dU_{hys}}{d\varepsilon_{max}} = U_{xl}\nu_e \quad (4)$$

Table 1 shows the slope of U_{hys} versus ε_{max} curves, Young's modulus E, and the cross-link density ν_e of the hydrogels calculated using eq 3. By substituting ν_e and the slope of U_{hys} versus ε_{max} curves into eq 4, one may estimate the average dissociation energies U_{xl} of the noncovalent bonds in the

Table 1. Slope of U_{hys} vs ε_{Max} Plots, Young's Modulus E, Cross-Link Density ν_e, and the Average Dissociation Energy U_{xl} of Noncovalent Bonds in NC-DNA-5/4 and NC-5 Hydrogels[a]

hydrogel	$dU_{hys}/d\varepsilon_{max}$ kJ·m^{-3}	E/kPa	ν_e/mol·m^{-3}	U_{xl}/kJ·mol^{-1}
NC-DNA-5/4	7.6 (0.3)	20.7 (2.1)	2.8 (0.3)	2.7 (0.2)
NC-DNA-5/4 (after cycle)	14.0 (0.2)	36.7 (4.4)	4.9 (0.6)	2.9 (0.4)
NC-5	10.0 (0.3)	21.1 (1.2)	2.8 (0.2)	3.6 (0.3)

[a]The numbers in parentheses are the standard deviations.

DOI: 10.1021/acsami.8b00168
ACS Appl. Mater. Interfaces 2018, 10, 8296−8306

hydrogels, as compiled in the last column of Table 1. U_{xl} is 2.7 ± 0.2 kJ·mol^{-1} for NC-DNA-5/4, and it slightly increases to 2.9 ± 0.4 kJ·mol^{-1} after the thermal cycle, as compared to 3.6 ± 0.3 kJ·mol^{-1} for NC-5 hydrogel. Considering that the strengths of chemical bonds, hydrogen bonds, and van der Waals bonds are 360, 3.2, and 0.64 kJ·mol^{-1}, respectively,[48,55] the bond strength in the hydrogels is in the range of the hydrogen bonds, and it slightly decreases after the incorporation of ds-DNA into the NC hydrogel.

The quasi-reversible manner of dissociation of hydrogen bonds in NC-DNA hydrogels under stress suggests their self-healing abilities. Figure 8a shows the photographs of two NC-DNA-5/4 gel specimens, where one of them was colored for clarity. When the two gel samples were put into contact and allowed to stand at 90 °C for 30 min followed by cooling to room temperature, it was not possible to separate the two parts by stretching manually. Figure 8b shows the images during uniaxial tensile tests of the healed hydrogel sample, and Figure 8c shows the stress–strain curves of virgin (solid curves) and healed NC-DNA-5/4 hydrogels. After healing at 90 °C, the hydrogel breaks at a stretch ratio of 1130 ± 140, which is close to that of the virgin NC-DNA hydrogel (1350 ± 200). It is interesting to note that both the Young's modulus E and the fracture stress σ_f of the hydrogel significantly increase after its healing at 90 °C. For instance, E increases from 21 ± 2 to 30 ± 1 kPa and σ_f increases from 48 ± 6 to 81 ± 5 kPa after healing at 90 °C, corresponding to 140–170% healing efficiencies. Healing conducted at 80 °C resulted in 48 ± 6% healing efficiency with respect to both the stretch ratio at break and the fracture stress while the modulus could completely be recovered. This suggests that the enhanced mechanical strength of NC-DNA hydrogels healed at 90 °C is due to the increase of the modulus E and fracture stress σ_f of DNA-containing hydrogels as observed during the heating–cooling cycles (Figure 4). Indeed, no such an improvement was observed when the healing tests were conducted using NC-5 hydrogel prepared without DNA (Figure 8c). NC-5 hydrogel healed at 90 °C exhibited a healing efficiency of 60 ± 5% with respect to the fracture stress. As shown in Figure 5b, E and σ_f of virgin NC-5/4 hydrogel increase from 21 ± 2 to 37 ± 4 kPa and from 48 ± 6 to 82 ± 6 kPa, respectively, by simply heating to 90 °C and then cooling back to 25 °C. Thus, as compared to the mechanical properties of the virgin hydrogel subjected to thermal cycle, the actual healing efficiencies with respect to the modulus and fracture stress are 81 ± 10 and 99 ± 6%, respectively.

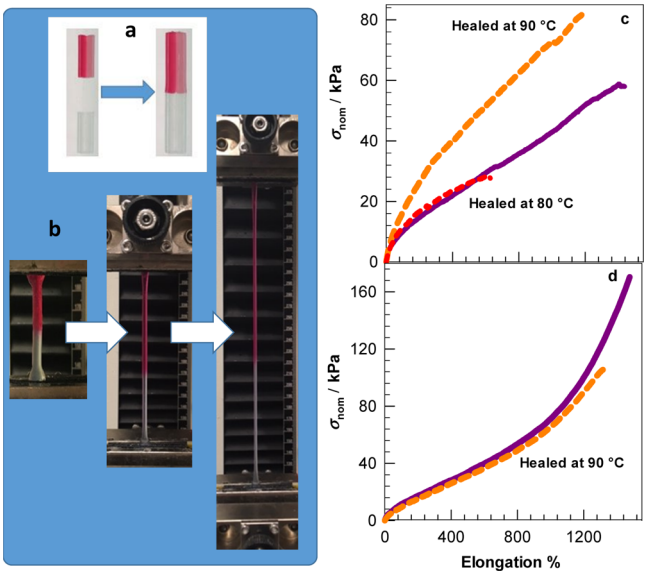

Figure 8. (a) Photographs of two NC-DNA-5/4 gel specimens, where one of them is colored for clarity. (b) Images of healed NC-DNA-5/4 hydrogel during uniaxial tensile tests. (c,d) Stress–strain curves of virgin (solid curves) and healed NC-DNA-5/4 (c) and NC-5 hydrogels (d).

Figure 9 shows the self-healing mechanism we propose for NC-DNA hydrogels. At the cut surface of a damaged gel sample at 24 °C, semiflexible ds-DNA fragments with a persistence length twice the diameter of Laponite nanoparticle behave as rigid segments, as shown in Figure 9a by ladderlike shapes. However, upon heating the joined cut surfaces above T_m, they dissociate and become flexible because of the much smaller persistence length of ss-DNA (Figure 9b).[56] Simultaneously, the mobility of the dissociated strands at the cut surface will significantly increase because the critical overlap

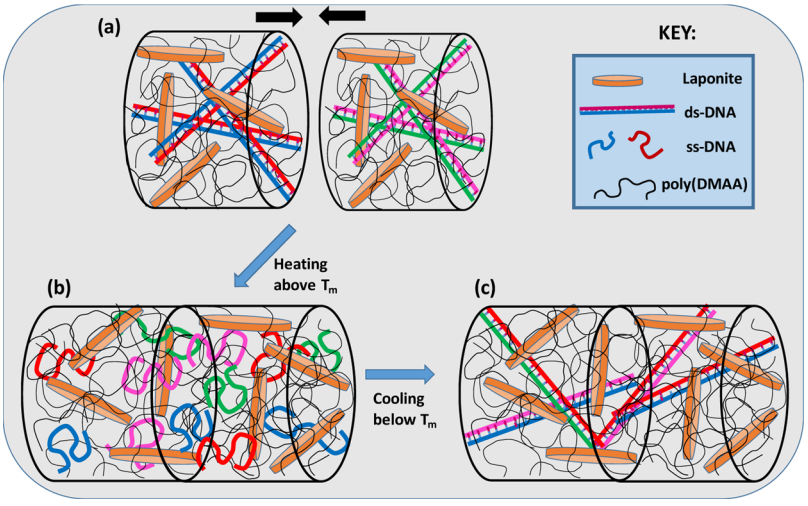

Figure 9. Cartoon showing cut surfaces of NC-DNA hydrogels (a), after pushing them into contact at above (b) and below T_m of ds-DNA (c). As a length scale, ds-DNA fragments behaving as a rigid segment are 50 nm in length, twice the diameter of Laponite nanoparticles.

DOI: 10.1021/acsami.8b00168
ACS Appl. Mater. Interfaces 2018, 10, 8296–8306

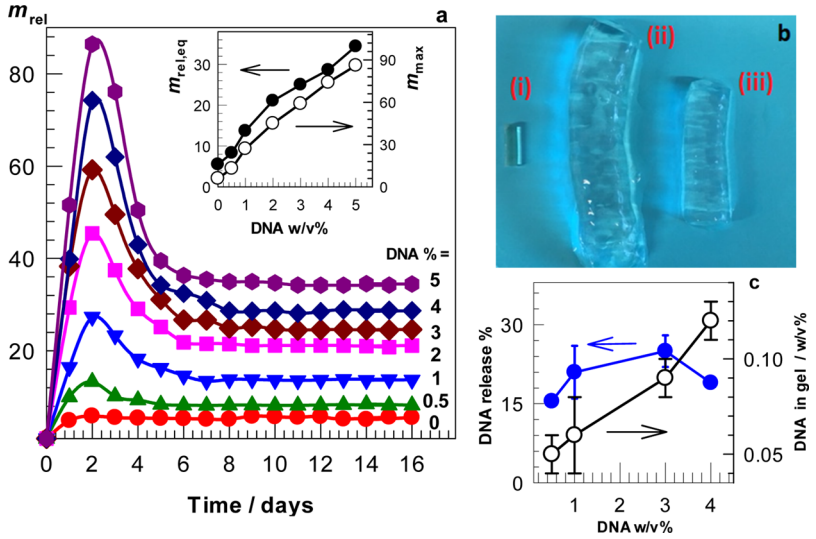

Figure 10. (a) Relative weight swelling ratio m_{rel} of NC-DNA-5/y hydrogels in water as a function of swelling time. DNA contents (y) are indicated. The inset shows the equilibrium $m_{rel,eq}$ (filled symbols) and maximum swelling ratios m_{max} (open symbols) of the hydrogels plotted against DNA w/v %. (b) Optical images of a NC-5/5 gel specimen just after preparation (i) and after maximum (ii) and equilibrium degrees of swelling in water (iii). (c) Released amount of DNA from NC-DNA hydrogels (filled circles) and DNA concentration in swollen hydrogels (open circles) both plotted against their initial DNA content y. The data are the average of the results from UV and fluorescence measurements.

concentration of DNA with 2000 base pairs 74-fold increases upon denaturation and becomes 3.2 w/v %, corresponding to the critical entanglement concentration of 6−9.3 w/v %.[27,28] Thus, the strands can move from one to another surface, whereas cooling back to room temperature enables the formation of bridges between the surfaces via base pairing between ss-DNA strands belonging to both surfaces, which facilitates healing process (Figure 9c).

All features of NC-DNA hydrogels discussed so far are related to their as-prepared states containing 88.5−93.5 wt % water. Figure 10a shows the typical swelling kinetics of NC-DNA-5/y hydrogels with various DNA contents (y), where the relative swelling ratio m_{rel} is plotted against the time of swelling. Immersion of the hydrogels in water results in a significant increase in their mass within 2 days, and after passing a maximum degree of swelling, they start to deswell until attaining an equilibrium degree of swelling. The inset of Figure 10a shows the equilibrium $m_{rel,eq}$ and maximum swelling ratios m_{max} of the hydrogels plotted against their initial DNA content y. The higher the DNA content of the hydrogels, the higher both the maximum and equilibrium degrees of swelling. For instance, Figure 10b shows the optical images of an NC-5/5 gel specimen at three states: as-prepared (i), maximum swelling (ii), and equilibrium swelling (iii). The gel mass first 86-fold increases but then decreases to attain an equilibrium swelling ratio of 34.

This swelling profile suggests that ds-DNA in the hydrogels partially releases during the initial swelling process. Thus, NC-DNA hydrogel initially behaves as a polyelectrolyte hydrogel because of the osmotic pressure of phosphate counterions of DNA and attains a large swelling ratio. However, as the DNA is gradually released from the hydrogel, the ionic osmotic pressure reduces so that the hydrogel progressively changes into a less ionic hydrogel with a distinctly reduced swelling ratio. Increasing equilibrium swelling ratio $m_{rel,eq}$ with increasing DNA content y indicates that a larger amount of DNA can be entrapped within the gel network in equilibrium with water as the DNA concentration at the gel preparation is increased. This was indeed observed. Figure 10c shows the released amount of DNA with respect to its initial amount at the gel preparation (filled symbols) and DNA concentration in swollen NC-DNA-5/y hydrogels (open symbols) plotted against the initial DNA content y. The released amount of DNA from NC-DNA-5/y hydrogels is 20 ± 4%, which is almost independent on y, whereas the concentration of DNA in equilibrium swollen hydrogels increases from 0.05 to 0.12 w/v % with increasing DNA content at the gel preparation. This DNA release behavior may provide applications of NC-DNA hydrogels as DNA carriers in gene therapy methods.

CONCLUSIONS

The hydrogels containing DNA in the protective environment of clay nanoparticles are excellent candidates to utilize the characteristics of DNA, such as bioresponsivity, biocompatibility, biodegradability, selective binding, and molecular recognition. We presented here novel DNA/clay hydrogels of high stretchability (up to 1500%) and a tensile strength between 20 and 150 kPa prepared by in situ polymerization of DMAA in aqueous solutions of ds-DNA (2−8 w/v %) in the presence of Laponite nanoparticles. Fluorescence measurements show that ds-DNA molecules in the gel network undergo thermal denaturation/renaturation cycles, leading to further improvement in the mechanical properties of the hydrogels. It was found that clay nanoparticles act like a chemical cross-linker and promote the elastic behavior of the hydrogels, whereas DNA contributes to their viscoelastic energy dissipation. The results of cyclic rheological and tensile tests indicate a quasi-reversible manner of dissociation and reformation of intermolecular bonds in the hydrogels. The strength of intermolecular bonds in DNA/clay hydrogels calculated from the hysteresis energies is in the range of the bond strength of hydrogen bonds. The hydrogels have the ability to self-heal, which is induced by heating the damaged gel samples above the melting temperature of ds-DNA, with a healing efficiency greater than 100%. For instance, after healing at 90 °C, the Young's modulus E and the fracture stress σ_f of

DOI: 10.1021/acsami.8b00168
ACS Appl. Mater. Interfaces 2018, 10, 8296−8306

the hydrogel increase from 21 ± 2 to 30 ± 1 kPa and from 48 ± 6 to 81 ± 5 kPa, respectively, corresponding to 140−170% healing efficiencies. The enhanced mechanical strength of the hydrogels healed at 90 °C is due to the modulus rise in hydrogels as observed during the heating−cooling cycles. Comparing the healed and virgin hydrogels, both heated to 90 °C and cooled back to 25 °C, the actual healing efficiencies with respect to the modulus and fracture stress are 81 ± 10 and 99 ± 6%, respectively.

■ ASSOCIATED CONTENT

Supporting Information

The Supporting Information is available free of charge on the ACS Publications website at DOI: 10.1021/acsami.8b00168.

Experimental details including synthesis, sample preparation, and characterization (PDF)

■ AUTHOR INFORMATION

Corresponding Authors

*E-mail: oguney@itu.edu.tr (O.G.).
*E-mail: okayo@itu.edu.tr (O.O.).

ORCID

Ahmet T. Uzumcu: 0000-0002-2440-5518
Oguz Okay: 0000-0003-2717-4150

Notes

The authors declare no competing financial interest.

■ ACKNOWLEDGMENTS

This work was supported by Istanbul Technical University (ITU), BAP 39773. O.O. thanks Turkish Academy of Sciences (TUBA) for the partial support.

■ REFERENCES

(1) Xu, J.; La Bean, T. H.; Craig, S. L. DNA Structures and their Applications in Nanotechnology. In *Supramolecular Polymers*; Ciferri, A., Ed.; CRC Press: Boca Raton, FL, 2004; pp 445−480.

(2) Bloomfield, V. A.; Crothers, D. M.; Tinoco, I., Jr. *Nucleic Acids: Structures, Properties, and Functions*; University Science Books: Sausalito, 2000.

(3) Shao, Y.; Jia, H.; Cao, T.; Liu, D. Supramolecular Hydrogels Based on DNA Self-Assembly. *Acc. Chem. Res.* **2017**, *50*, 659−668.

(4) Wang, D.; Hu, Y.; Liu, P.; Luo, D. Bioresponsive DNA Hydrogels: Beyond the Conventional Stimuli Responsiveness. *Acc. Chem. Res.* **2017**, *50*, 733−739.

(5) Okay, O. DNA Hydrogels: New Functional Soft Materials. *J. Polym. Sci., Part B: Polym. Phys.* **2011**, *49*, 551−556.

(6) Alemdaroglu, F. E.; Herrmann, A. DNA meets Synthetic Polymers—Highly Versatile Hybrid Materials. *Org. Biomol. Chem.* **2007**, *5*, 1311−1320.

(7) Murakami, Y.; Maeda, M. DNA-Responsive Hydrogels that can Shrink or Swell. *Biomacromolecules* **2005**, *6*, 2927−2929.

(8) Ishizuka, N.; Hashimoto, Y.; Matsuo, Y.; Ijiro, K. Highly Expansive DNA Hydrogel Films Prepared with Photocrosslinkable Poly(vinyl alcohol). *Colloids Surf., A* **2006**, *284−285*, 440−443.

(9) Lilienthal, S.; Shpilt, Z.; Wang, F.; Orbach, R.; Willner, I. Programmed DNAzyme-Triggered Dissolution of DNA-Based Hydrogels: Means for Controlled Release of Biocatalysts and for the Activation of Enzyme Cascades. *ACS Appl. Mater. Interfaces* **2015**, *7*, 8923−8931.

(10) Kang, H.; Liu, H.; Zhang, X.; Yan, J.; Zhu, Z.; Peng, L.; Yang, H.; Kim, Y.; Tan, W. Photoresponsive DNA-Cross-linked Hydrogels for Controllable Release and Cancer Therapy. *Langmuir* **2011**, *27*, 399−408.

(11) Xiang, B.; He, K.; Zhu, R.; Liu, Z.; Zeng, S.; Huang, Y.; Nie, Z.; Yao, S. Self-Assembled DNA Hydrogel Based on Enzymatically Polymerized DNA for Protein Encapsulation and Enzyme/DNAzyme Hybrid Cascade Reaction. *ACS Appl. Mater. Interfaces* **2016**, *8*, 22801−22807.

(12) Jin, J.; Xing, Y.; Xi, Y.; Liu, X.; Zhou, T.; Ma, X.; Yang, Z.; Wang, S.; Liu, D. A Triggered DNA Hydrogel Cover to Envelop and Release Single Cells. *Adv. Mater.* **2013**, *25*, 4714−4717.

(13) Wang, Y.; Shao, Y.; Ma, X.; Zhou, B.; Faulkner-Jones, A.; Shu, W.; Liu, D. Constructing Tissuelike Complex Structures using Cell-Laden DNA Hydrogel Bricks. *ACS Appl. Mater. Interfaces* **2017**, *9*, 12311−12315.

(14) Joseph, K. A.; Dave, N.; Liu, J. Electrostatically Directed Visual Fluorescence Response of DNA-Functionalized Monolithic Hydrogels for Highly Sensitive Hg^{2+} Detection. *ACS Appl. Mater. Interfaces* **2011**, *3*, 733−739.

(15) Dave, N.; Chan, M. Y.; Huang, P.-J. J.; Smith, B. D.; Liu, J. Regenerable DNA-Functionalized Hydrogels for Ultrasensitive, Instrument-Free Mercury(II) Detection and Removal in Water. *J. Am. Chem. Soc.* **2010**, *132*, 12668−12673.

(16) Liu, D.; Jia, S.; Zhang, H.; Ma, Y.; Guan, Z.; Li, J.; Zhu, Z.; Ji, T.; Yang, C. J. Integrating Target-Responsive Hydrogel with Pressuremeter Readout Enables Simple, Sensitive, User-friendly, Quantitative point-of-care Testing. *ACS Appl. Mater. Interfaces* **2017**, *9*, 22252−22258.

(17) Baeissa, A.; Dave, N.; Smith, B. D.; Liu, J. DNA-Functionalized Monolithic Hydrogels and Gold Nanoparticles for Colorimetric DNA Detection. *ACS Appl. Mater. Interfaces* **2010**, *2*, 3594−3600.

(18) Xu, Y.; Wu, Q.; Sun, Y.; Bai, H.; Shi, G. Three-Dimensional Self-Assembly of Graphene Oxide and DNA into Multifunctional Hydrogels. *ACS Nano* **2010**, *4*, 7358−7362.

(19) Li, C.; Chen, P.; Shao, Y.; Zhou, X.; Wu, Y.; Yang, Z.; Li, Z.; Weil, T.; Liu, D. A Writable Polypeptide−DNA Hydrogel with Rationally Designed Multi-Modification Sites. *Small* **2015**, *9−10*, 1138−1143.

(20) Li, C.; Rowland, M. J.; Shao, Y.; Cao, T.; Chen, C.; Jia, H.; Zhou, X.; Yang, Z.; Scherman, O. A.; Liu, D. Responsive Double Network Hydrogels of Interpenetrating DNA and CB[8] Host−Guest Supramolecular Systems. *Adv. Mater.* **2015**, *27*, 3298−3304.

(21) Cheng, E.; Xing, Y.; Chen, P.; Yang, Y.; Sun, Y.; Zhou, D.; Xu, L.; Fan, Q.; Liu, D. A pH-Triggered, Fast-Responding DNA Hydrogel. *Angew. Chem., Int. Ed.* **2009**, *48*, 7660−7663.

(22) Kahn, J. S.; Hu, Y.; Willner, I. Stimuli-Responsive DNA-Based Hydrogels: From Basic Principles to Applications. *Acc. Chem. Res.* **2017**, *50*, 680−690.

(23) Lu, C.-H.; Guo, W.; Hu, Y.; Qi, X.-J.; Willner, I. Multitriggered Shape-Memory Acrylamide−DNA Hydrogels. *J. Am. Chem. Soc.* **2015**, *137*, 15723−15731.

(24) Um, S. H.; Lee, J. B.; Park, N.; Kwon, S. Y.; Umbach, C. C.; Luo, D. Enzyme-Catalysed Assembly of DNA Hydrogel. *Nat. Mater.* **2006**, *5*, 797−801.

(25) Tanaka, S.; Wakabayashi, K.; Fukushima, K.; Yukami, S.; Maezawa, R.; Takeda, Y.; Tatsumi, K.; Ohya, Y.; Kuzuya, A. Intelligent, Biodegradable, and Self-Healing Hydrogels Utilizing DNA Quadruplexes. *Chem.—Asian J.* **2017**, *12*, 2388−2392.

(26) Xing, Y.; Cheng, E.; Yang, Y.; Chen, P.; Zhang, T.; Sun, Y.; Yang, Z.; Liu, D. Self-Assembled DNA Hydrogels with Designable Thermal and Enzymatic Responsiveness. *Adv. Mater.* **2011**, *23*, 1117−1121.

(27) Topuz, F.; Okay, O. Rheological Behavior of Responsive DNA Hydrogels. *Macromolecules* **2008**, *41*, 8847−8854.

(28) Topuz, F.; Okay, O. Formation of Hydrogels by Simultaneous Denaturation and Cross-linking of DNA. *Biomacromolecules* **2009**, *10*, 2652−2661.

(29) Yang, D.; Peng, S.; Hartman, M. R.; Gupton-Campolongo, T.; Rice, E. J.; Chang, A. K.; Gu, Z.; Lu, G. Q.; Luo, D. Enhanced Transcription and Translation in Clay Hydrogel and Implications for Early Life Evolution. *Sci. Rep.* **2013**, *3*, 3165.

DOI: 10.1021/acsami.8b00168
ACS Appl. Mater. Interfaces 2018, 10, 8296−8306

(30) Cai, P.; Huang, Q.-Y.; Zhang, X.-W. Interactions of DNA with Clay Minerals and Soil Colloidal Particles and Protection Against Degradation by DNase. *Environ. Sci. Technol.* **2006**, *40*, 2971−2976.
(31) Haraguchi, K.; Takehisa, T. Nanocomposite Hydrogels: A Unique Organic−Inorganic Network Structure with Extraordinary Mechanical, Optical, and Swelling/De-swelling Properties. *Adv. Mater.* **2002**, *14*, 1120−1124.
(32) Haraguchi, K.; Takehisa, T.; Fan, S. Effects of Clay Content on the Properties of Nanocomposite Hydrogels Composed of Poly(N-isopropylacrylamide) and Clay. *Macromolecules* **2002**, *35*, 10162−10171.
(33) Haraguchi, K.; Farnworth, R.; Ohbayashi, A.; Takehisa, T. Compositional Effects on Mechanical Properties of Nanocomposite Hydrogels Composed of Poly(N,N-dimethylacrylamide) and Clay. *Macromolecules* **2003**, *36*, 5732−5741.
(34) Haraguchi, K.; Li, H.-J.; Matsuda, K.; Takehisa, T.; Elliott, E. Mechanism of Forming Organic/Inorganic Network Structures During In-situ Free-radical Polymerization in PNIPA−Clay Nanocomposite Hydrogels. *Macromolecules* **2005**, *38*, 3482−3490.
(35) Taki, A.; John, B.; Arakawa, S.; Okamoto, M. Structure and Rheology of Nanocomposite Hydrogels Composed of DNA and Clay. *Eur. Polym. J.* **2013**, *49*, 923−931.
(36) Uzumcu, A. T.; Guney, O.; Okay, O. Nanocomposite DNA Hydrogels with Temperature Sensitivity. *Polymer* **2016**, *100*, 169−178.
(37) Uemura, Y.; McNulty, J.; Macdonald, P. M. Associative Behavior and Diffusion Coefficients of Hydrophobically Modified Poly(N,N-dimethylacrylamides). *Macromolecules* **1995**, *28*, 4150−4158.
(38) Relógio, P.; Martinho, J. M. G.; Farinha, J. P. S. Effect of Surfactant on the Intra- and Intermolecular Association of Hydrophobically Modified Poly(N,N-dimethylacrylamide). *Macromolecules* **2005**, *38*, 10799−10811.
(39) Mongondry, P.; Tassin, J. F.; Nicolai, T. Revised State Diagram of Laponite Dispersions. *J. Colloid Interface Sci.* **2005**, *283*, 397−405.
(40) Mongondry, P.; Nicolai, T.; Tassin, J.-F. Influence of Pyrophosphate or Polyethylene oxide on the Aggregation and Gelation of Aqueous Laponite Dispersions. *J. Colloid Interface Sci.* **2004**, *275*, 191−196.
(41) Klein, A.; Whitten, P. G.; Resch, K.; Pinter, G. Nanocomposite Hydrogels: Fracture Toughness and Energy Dissipation Mechanisms. *J. Polym. Sci., Part B: Polym. Phys.* **2015**, *53*, 1763−1773.
(42) Okay, O.; Oppermann, W. Polyacrylamide−Clay Nanocomposite Hydrogels: Rheological and Light Scattering Characterization. *Macromolecules* **2007**, *40*, 3378−3387.
(43) Haraguchi, K.; Uyama, K.; Tanimoto, H. Self-Healing in Nanocomposite Hydrogels. *Macromol. Rapid Commun.* **2011**, *32*, 1253−1258.
(44) Karacan, P.; Okay, O. Ethidium Bromide Binding to DNA Cryogels. *React. Funct. Polym.* **2013**, *73*, 442−450.
(45) Cosa, G.; Focsaneanu, K.-S.; McLean, J. R. N.; McNamee, J. P.; Scaiano, J. C. Photophysical Properties of Fluorescent DNA-Dyes Bound to Single- and Double-Stranded DNA in Aqueous Buffered Solution. *Photochem. Photobiol.* **2001**, *73*, 585−599.
(46) Ma, Y.; Zhang, G.; Pan, J. Spectroscopic Studies of DNA Interactions with Food Colorant Indigo Carmine with the Use of Ethidium Bromide as a Fluorescence Probe. *J. Agric. Food Chem.* **2012**, *60*, 10867−10875.
(47) Orakdogen, N.; Erman, B.; Okay, O. Evidence of Strain Hardening in DNA Gels. *Macromolecules* **2010**, *43*, 1530−1538.
(48) Webber, R. E.; Creton, C.; Brown, H. R.; Gong, J. P. Large Strain Hysteresis and Mullins Effect of Tough Double-Network Hydrogels. *Macromolecules* **2007**, *40*, 2919−2927.
(49) Lake, G. J.; Thomas, A. G. The Strength of Highly Elastic Materials. *Proc. R. Soc. London, Ser. A* **1967**, *300*, 108−119.
(50) Okay, O. Self-Healing Hydrogels Formed via Hydrophobic Interactions. *Adv. Polym. Sci.* **2015**, *268*, 101−142.
(51) Tang, J.; Chen, X.; Pei, Y.; Fang, D. Pseudoelasticity and Nonideal Mullins Effect of Nanocomposite Hydrogels. *J. Appl. Mech.* **2016**, *83*, 111010.
(52) Flory, P. J. *Principles of Polymer Chemistry*; Cornell University Press: Ithaca, NY, 1953.
(53) Treloar, L. R. G. *The Physics of Rubber Elasticity*; University Press: Oxford, 1975.
(54) Tuncaboylu, D. C.; Sahin, M.; Argun, A.; Oppermann, W.; Okay, O. Dynamics and Large Strain Behavior of Self-Healing Hydrogels with and without Surfactants. *Macromolecules* **2012**, *45*, 1991−2000.
(55) Dion, M.; Rydberg, H.; Schröder, E.; Langreth, D. C.; Lundqvist, B. I. Van der Waals Density Functional for General Geometries. *Phys. Rev. Lett.* **2004**, *92*, 246401.
(56) Pan, W.; Wen, H.; Niu, L.; Su, C.; Liu, C.; Zhao, J.; Mao, C.; Liang, D. Effects of Chain Flexibility on the Properties of DNA Hydrogels. *Soft Matter* **2016**, *12*, 5537−5541.

DOI: 10.1021/acsami.8b00168
ACS Appl. Mater. Interfaces 2018, 10, 8296−8306